UNSTEADY TWO-DIMENSIONAL STUDY OF AIR FLOW IN A POROUS CONFINED SPACE : APPLICATION IN ELECTRONIC DEVICE

Dalila MENACER*1, Mohammed Choukri Korti1, Lakhdar Saihi1, Youcef Sahli1

[1]Unité de Recherche en Energies Renouvelables en Milieu Saharien, URERMS, Centre de Développement des Energies Renouvelables, CDER 01000, Adrar, Algeria

*Corresponding author; E-mail: menacerdalila2018@gmail.com / m.dalila@urerms.cder.dz

In this work, the mechanism instability of heat transfer and fluid flow across an electronic device has been conducted in anunsteady two-dimensional environment.The pore structure has a constant central heat source Th at below and has been cooled with lower temperature Tc from its vertical sides moved upper ward with constant velocity V_0, while the other walls were considered to be thermally insulated.The governing equations of a Darcy-Brinkman-Forchheimer have been adopted, they are discretized using the finite difference method for non-uniform grids and numerically solved employing Runge-Kutta fourth-order method.The principal objective of this contribution is the investigation of the impact of moving boundaries on the occurrence of thermal and dynamical instabilities in the porous space using partial heating at the bottom. The calculations have been carried out with porosity approaching 1 and a series of mixed convection parameters bounded by 0.5 and 35. Reynolds and Prandtl numbers, along with Darcy's value, have been fixed respectively to 100, 0.71, and 0.1. The obtained results have shown that at different time stations, interesting disturbances in the stability of flow have been provided in the current work. Thus, five different flow structures were highlighted depending on the Richardson number. The employed model can be useful for describing the physical behaviors of cooling of the electronic components present in almost all devices.

Keywords*: non-uniform grids, instability, pore-structure, Darcy Brinkman-Forchheimer type, different sructures*

1. Introduction

The problem of heat exchange and fluid dynamics in porous mediums is among the current research trends in a huge number of fields, such as the transport of pollutants in groundwater, soil remediation, oil and gaz extraction, drying, the semiconductor industry, the thermal design of the building, the behavior of certain parts of a nuclear reactor and cooling electronic and electrotechnic components, …etc. In biological processes in the human body [1].It also plays a major role in the stability of geologically sequestered CO_2[2] and contributes to mixed convective heat transfer over a solar captor for clean energy production. The theory of perturbation has been developed to study the effects of gravity modulation and internal heating through a porous layer by Akhila et al. [3]. It has been shown that cell eccentricity, Darcy, and Rayleigh parameters have a significant influence on heat transport. Roy et al. [4] performed numerical simulations of the flow of free-forced convective hybrid nanofluids over a shrinkable porous cylinder, revealing that the thermal boundary layer of each component with water is narrower than that of the entire mixture. Aly et al. [5] studied the natural motion of Al_2O_3 for three distinctive structures inside a porous cylindrical shape based on the ISPH procedure, highlighting clear differences in velocity values and isotherm fields for different structures. Using the finite element method, Abderrahmane et al. [6] examined mixed convective flow in a porous medium-filled trapezoidal cavity and found that higher Darcy number values improve the heat transmission rate. Mourad et al. [7] explored numerically the laminar and natural flow of Cu/H_2O nanofluid in a porous ring formed by a Koch snowflake, revealing that increasing Rayleigh numbers lead to higher intensity of heat transfer inside the annulus. Choudhary et al. [8] investigated three different heights of a heat source below a corrugated enclosure saturated with a porous medium using the finite difference approach, discovering that the thickness of the thermal boundary layer changes depending on the type of vortex formed at the heated area. Xuan et al. [9] thoroughly examined the effects of porosity, thermal conductivity, and heating direction on the critical pore size that allows natural convection, demonstrating that lower boundary heating plays an important role compared to thermal heating of the vertical sides. Virupaksha et al. [10] applied CNNs model to investigate free convection in a heterogeneous porous cavity and found that the ED-CNN approach is more effective than the Deep Neural Network in allowing the time evolution of flow behavior. Bazneshin et al. [11] conducted a numerical study to identify factors affecting the efficiency of latent energy storage based on phase change material, revealing that the insertion of a porous structure into the pipe improved the capacity of the phase change system by 93%. Rasool et al. [12] used the finite element approach to study the transport of carbon nanoparticles in a Z-staggered cavity by water flow, observing that increasing Reynolds number decreased the vertical velocity along the centerline of the cavity. Ashraf et al. [13] reviewed an oscillatory mixed convective process through a cylindrical configuration embedded in a porous medium, finding that transient heat flow and pattern fields are related to the amplitude and phase angle. Chakkingal et al. [14] discussed the influence of the height and location of packing layers on heat and fluid mechanisms numerically using Ansys-Fluent, revealing differences in heat transfer rates for higher Rayleigh values regardless of the location and number of porous layers. Luther et al. [15] reported on the role of inclination on the stability of transient convective flow and concentration field in a porous layer, observing that onset perturbations were obtained for ($90° \leq \theta \leq 180°$). Kumar et al. [16] documented the thermal stabilization of a swimmer subjected to high vibration using the Darcy model, finding that the stabilization nature of the flow broke with increasing gyrotactic propulsion. Dalila et al. [17] numerically analyzed the role of moving sides on the nature of convective flow in a partially heated cavity filled with a porous medium, noting that dynamic fields remained almost similar for lower Darcy values of 0.001 and 0.01.In this context, several scientific contributions related to hybrid systems have been made such as the effect of porous media on a three-dimensional photovoltaic system performance which has been simulated by Sangtarash et al. [18]. It was found that the wood is the better material for use in middle configuration but the graphite is not recommended for leads to the smallest thermal efficiency for the full configuration at the middle one. The impact of using porous materials on the improvement of PV solar systems efficiency has been investigated in the article of Meria et al. [19]. The findings shows that adding of porous device improved the energy efficiency from 10% to 28% while a drop in temperature of the phoovoltaïc cell from 5 to 25 degrees Celsius was observed. A wavy-walled cavity filled with an hybrid nanofluid involving permeable systems was examined numerically in the paper of Mandal et al. [20]. The results reveal an improvement in heat transfer of 261.49% at higher frequencies.In addition, higher nanoparticle concentrations result in reduced the flow strength. Mass and heat transfer applications in non-Newtonian fluids have drawn a lot of interest in the literature [21]. The authors analyzed the porosity and the magnetohydrodynamique Impact on the heat transfer in a permeable cone applying the finite difference technique. It's noticed that the incorporation of magnetohydrodynamics and porosity effects increases the rate of heat exchange and microorganism diffusion. Employing MATLAB with bvp4c method, Zaman et al. [22] studied the boundary layer approximation of nanofuid over a slender cylindrical shape. They found that increasing the fluid parameter, the velocity profile will rise while the the Brownian motion and Prandtl number lessen the temperature profile.

The primary objective of this study is to provide a numerical solution for understanding the effects of convective regimes on the stability of airflow in a porous substrate by introducing a heat source at the center of the bottom. The sliding lids are moved against the direction of the buoyancy current. This document has highlighted the unstable, complex, and disorderly nature of the bifurcation phenomenon. This model is also applicable in many industrial processes such as heating, air conditioning, and cooling of electrical and electronic components to protect them from heat dissipation due to their need for higher power. Improving the cooling of these electronic boxes requires the injection of airflow through the side walls at lower temperatures.

2. Problem description and numerical procedure

2.1. Problem description

A two-dimensional cell is considered, with moving lids embedded in a homogeneous porous material. The lower boundary was heated using a source of size l=4/5L, assumed to be heated at a high temperature T_h, while all remaining parts of the system were considered thermally insulated. The geometric configuration is depicted in Fig. 1.

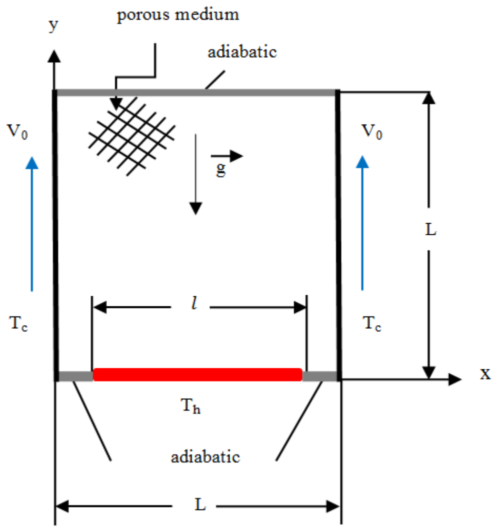

Fig 1. Diagram of the considered problem

2.2. Numerical formulation

The non-dimentional Navier-Stokes equations describing the flow dynamics in a 2-D cell are expressed as:

Continuity equation

$$\frac{\partial U}{\partial X} + \frac{\partial V}{\partial Y} = 0 \tag{1}$$

Momentum equation

The Darcy-Brinkman-Forchheimer model can be written as follows:

$$\frac{\rho_f}{\varphi}\left[\frac{\partial \vec{V}}{\partial t} + \frac{1}{\varphi}\left(\vec{V}.\nabla\right)\vec{V}\right] = -\nabla(P) + \rho_f \vec{g} - \frac{\mu}{K}\vec{V} + \frac{\mu}{\varphi}\nabla^2\vec{V} - \frac{C_F \rho_f}{K^{1/2}}\left|\vec{V}\right|\vec{V} \qquad [18](2)$$

With:

$$C_F = \frac{1.75}{\sqrt{150 Da \varphi}} \text{and } \left|\vec{V}\right| = \sqrt{U^2 + V^2}$$

Energy equation

$$\frac{\partial \theta}{\partial \tau} + U\frac{\partial \theta}{\partial X} + V\frac{\partial \theta}{\partial Y} = \frac{1}{RePr}\left(\frac{\partial^2 \theta}{\partial X^2} + \frac{\partial^2 \theta}{\partial Y^2}\right) \tag{3}$$

The velocity components are:

$$U = \frac{\partial \psi}{\partial Y} \, and \; V = -\frac{\partial \psi}{\partial X} \tag{4}$$

Vorticity equation

$$\frac{\partial \mathrm{\omega}}{\partial \mathrm{\tau}} + \frac{1}{\mathrm{\varphi}}\left(\mathrm{U}\frac{\partial \mathrm{\omega}}{\partial \mathrm{X}} + \mathrm{V}\frac{\partial \mathrm{\omega}}{\partial \mathrm{Y}}\right) = \mathrm{\varphi}\left(-\frac{1}{\mathrm{ReDa}} - \mathrm{C_F}\left|\vec{\mathrm{V}}\right|\right)\mathrm{\omega} - \mathrm{C_F}\left(\mathrm{V}\frac{\partial\left|\vec{\mathrm{V}}\right|}{\partial \mathrm{X}} - \mathrm{U}\frac{\partial\left|\vec{\mathrm{V}}\right|}{\partial \mathrm{Y}}\right) + \frac{1}{\mathrm{Re}}\left(\frac{\partial^2 \mathrm{\omega}}{\partial \mathrm{X}^2} + \frac{\partial^2 \mathrm{\omega}}{\partial \mathrm{Y}^2}\right) + \mathrm{\varphi Ri}\frac{\partial \mathrm{\theta}}{\partial \mathrm{X}} \tag{5}$$

Stream-function equation

$$\frac{\partial^2 \psi}{\partial X^2} + \frac{\partial^2 \psi}{\partial Y^2} = -\omega \tag{6}$$

Prandtl, Reynolds, Grashof, Richardson, and Darcy numbers are respectively defined by the following expressions:

$$Pr = \frac{\nu}{\alpha_e}, Re = \frac{V_0 L}{\nu}, Gr = \frac{g\beta L(T_c - T_f)L^3}{\nu^2}, Ri = \frac{Gr}{Re^2} \; and \;\; Da = \frac{k}{L^2} \tag{7}$$

Dimensionless parameters are expressed by the following relations:

$$X = \frac{x}{L}, Y = \frac{\mathrm{y}}{L}, U = \frac{u}{V_0}, V = \frac{\mathrm{v}}{V_0}, \tau = t\frac{V_0}{L}, \theta = \frac{(T - T_c)}{(T_\mathrm{h} - T_c)}, \omega = \frac{\Omega L}{V_0} \; and \; \psi = \frac{\Psi}{L V_0} \tag{8}$$

The average Nusselt number is defined as

$$\overline{Nu} = \frac{1}{\varepsilon}\int_{0}^{\varepsilon} -\frac{\partial\theta}{\partial X}\bigg|_{Y=0} dX \tag{9}$$

The resolution of the system equations obtained previously requires the incorporation of the following initial conditions:

Initially, the fluid is reset. Eq. (10).

$$At\ \tau = 0{:}\ \theta = 0, \qquad U = 0\ and\ V = 0 \tag{10}$$

The appropriate boundary conditions are:

$$\theta = 0 \quad U = 0 \quad V = 1\ at \begin{cases} X = 0 \\ X = 1 \end{cases} and\ 0 < Y < 1 \tag{11}$$

$$\theta = 1 \quad U = V = 0\ atY = 0\ and\ \frac{1-\varepsilon}{2} \le X \le \frac{1+\varepsilon}{2} \tag{12}$$

$$\frac{\partial\theta}{\partial Y} = 0 \quad V = 0\ at\ Y = 0\ and\ 0 < X < \frac{1-\varepsilon}{2}\ , \qquad \frac{1+\varepsilon}{2} < X < 1 \tag{13}$$

$$\frac{\partial\theta}{\partial Y} = 0 \quad U = V = 0\ at\ Y = 1\ and\ 0 < X < 1 \tag{14}$$

The boundary conditions of the vorticity can be evaluated from Eq.6 according to the following expressions:

$$\omega_{1,j} = \frac{2\left[\psi_{(1,j)} - \psi_{(2,j)} - V_0 \Delta X_1\right]}{{\Delta X_1}^2} \tag{15}$$

$$\omega_{nxt,j} = \frac{2\left[\psi_{(nxt,j)} - \psi_{(nxt-1,j)} + V_0 \Delta X_{nxt-1}\right]}{{\Delta X_{nxt-1}}^2} \tag{16}$$

$$\omega_{i,1} = \frac{2\left[\psi_{(i,1)} - \psi_{(i,2)}\right]}{{\Delta Y_1}^2} \tag{17}$$

$$\omega_{i,nyt} = \frac{2\left[\psi_{(i,nyt)} - \psi_{(i,nyt-1)}\right]}{{\Delta Y_{nyt-1}}^2} \tag{18}$$

2.3. Numerical procedure

The obtained system of energy and vorticity equations with corresponding boundary conditions was resolved based on finite differences. The discretization of the source term of the energy equation and velocities, along with the diffusive terms, has been achieved employing fourth-order central differencing. The fourth-order Runge-Kutta method has been adopted for the time stepping of temporal terms. A third-order Upwind scheme [23] has been chosen for the convective terms. Converged solutions of the stream function at each time step have been ensured using an iterative procedure (N.L.O.R) [24].

2.4. Grid independence study

The computation details of typical grid refinement on the heat transfer rate for various Darcy numbers are presented in the Table. 1. It should be noted that the independence of the grid system is achieved when using a non-uniform mesh of size equal to 101x101 for all subsequent simulations. This choice is made because the maximum relative error obtained from this grid resolution is in the order of 1% compared to the structure dimension of 201x201. Moreover, this decision is also motivated by the balance between precision and available CPU time.

Table. 1

Grid refinement effects on the rate of heat exchange at various Darcy number

Darcy number	Grid				
	61x61	**81x81**	**101x101**	**161x161**	**201x201**
Da=10-3	6.7279	6.8883	7.2006	7.2159	7.2173
$Da=10^{-2}$	14.6815	15.3231	15.1358	15.1364	15.1399
$Da=10^{-1}$	14.8832	15.4624	16.1195	16.1202	16.1217

2.5. Code validation and accuracy

A comparison of the results obtained with certain works cited in the literature was carried out. The first tests of current fields and isotherm contours shown in Fig. 2 are qualitatively in excellent agreement with those of Kumar et al. [25]. Then, the minimum and maximum values of the horizontal velocity across the vertical mid-plane (see Fig. 3) at $Ri=10^{-2}$ have been compared with those of this work. From the Table. 2, it can be seen that the obtained difference does not exceed 3.83%. As can be noticed from these tests, the present numerical procedure shows excellent agreement between the two cases.

Table. 2

Comparison of the obtained minimum and maximum values of the two horizontal and vertical velocities respectively along the midplane from the present solution and that of Iwatsu[26], Khanafer [27] and Waheed [28] at $Gr=10^2$ and $Re=10^2$

Darcy number	Present work	Iwatsu	Khanafer	Waheed	Error %
U_{min}	-0.2169	-0.2037	-0.2122	-0.21198	2.21
U_{max}	1.000	1.000	1.000	1.000	-
V_{min}	-0.2354	-0.2448	-0.2506	-0.25107	3.83
V_{max}	0.1761	0.1699	0.1765	0.177125	0.22

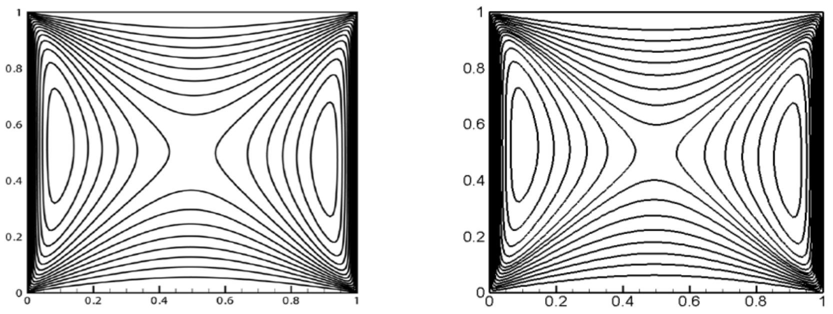

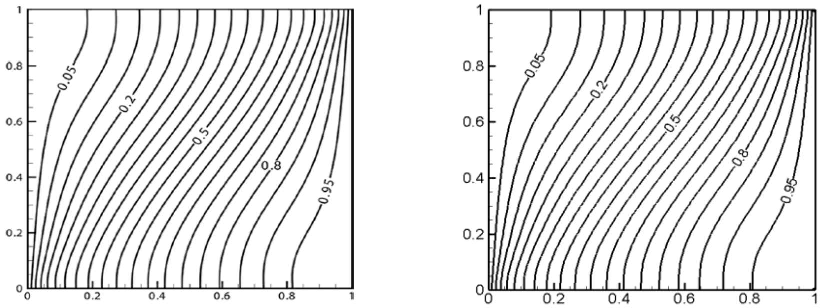

Fig1. Pattern fields (top) and temperature distributions (lower row) from Kumar et al. [25] (left) and the present model (right) at φ=0.9, $Gr=10^4$ and $Re=10^3$

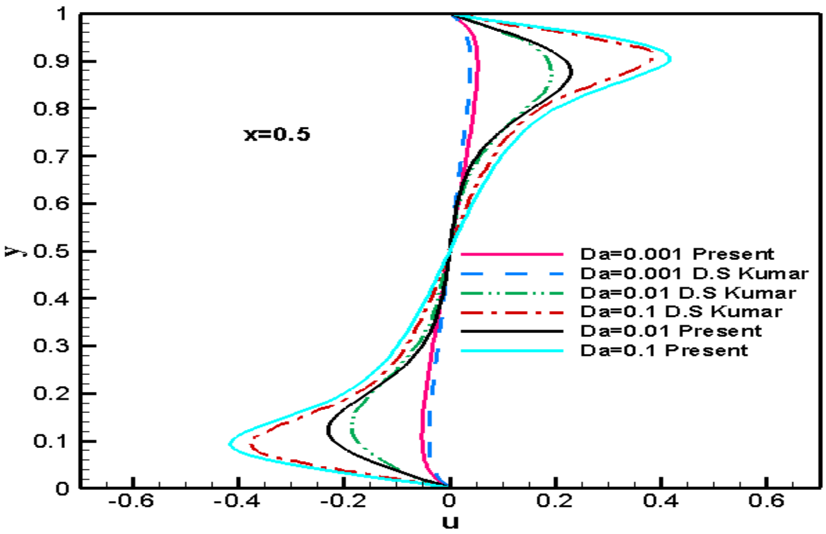

Fig 3. Comparison of the obtained horizontal velocity along the vertical center line with those of the work [25] at φ=0.9, $Gr=10^4$ and $Re=10^3$

3. Results and discussion

The flow presented by this model involving both free and forced convection commonly which called mixed convection. Thus, the Richardson number is chosen as the bifurcation parameter because it allows us to define the relative importance of these two modes of heat transfer inside the cavity. In this section, our goal is to predict the different critical values of Darcy and Richardson numbers throughout a range $0.5 \leq \mathrm{Ri} \leq 35$ for the occurrence of flow instability and bifurcations inside the square porous enclosure with moving lids and heating from below. These operating conditions have been chosen to obtain an asymmetric flow structure, taking into consideration perfectly symmetric boundary conditions for the physical system under consideration. The Darcy parameter was set to 0.1, corresponding to very high permeability, for which the behavior of the porous medium is close to that of a pure fluid. The length ratio of the heated part is equal to 4/5. All computations performed here are carried out with a very small time step on the order of 2.10^{-5}. The Grashoff number was varied in the runge from 5.10^3 to 35.10^4.

3.1. Effect of Richardson number when *Da*=0.1

The scope of the influence of increasing Richardson value on the average Nusselt number is investigated and discussed in this section. The numerical tests have permitted us to observe five completely different flow circulations according to the value of this parameter, which are highlighted in Fig. 5 by the captures of the stream functions and temperature distributions.

The flow details of this problem are depicted in Fig. 4. The first type, characterized by a flow formed by two counter-rotating and perfectly identical cells, is obtained for Richardson numbers whose value is between 0.5 and 6.8. An increment in this parameter to a first critical value equal to 11.76, results in the flow still being characterized by two counter-rotating but unsymmetrical cells. For a value of 11.77 (a difference of 0.1) of this number, we observe a sudden drop in the average Nusselt number and a flow type defined by four symmetrical cells. This last flow is maintained up to a second critical value of the Richardson number equal to 22.7. When this number becomes equivalent to 22.8 (a difference of 0.1), we notice a clear increase in the Nusselt number, and we return to a non-symmetrical two-cell flow, which is maintained until a third critical value of Richardson equal to 25.9. Beyond this value, the previous structure transitions to another characterized by two pairs of symmetrical cells.

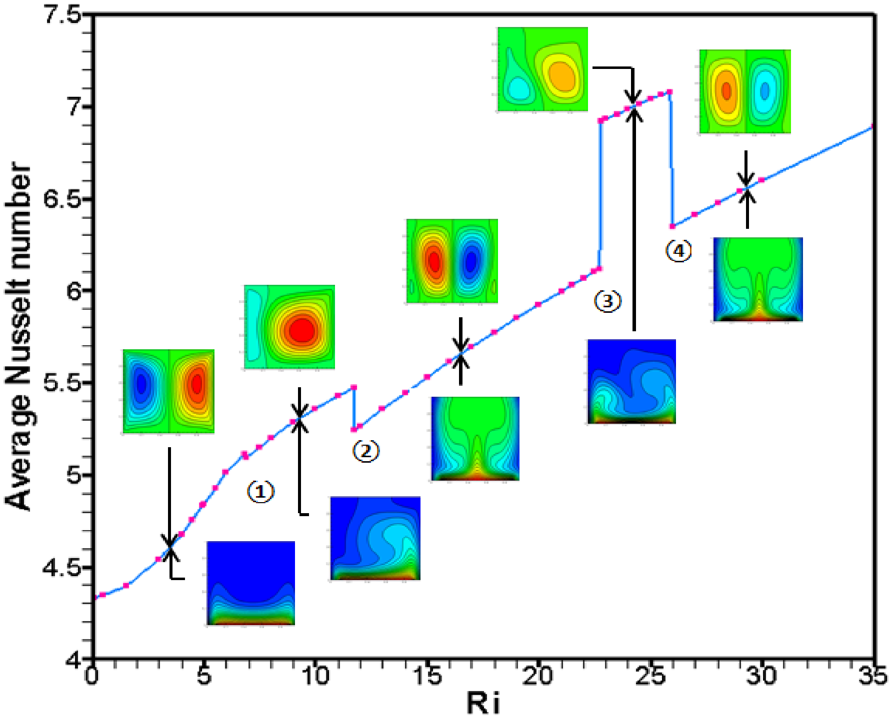

Fig 4. Effect of Richardson's value on the heat transfer rate.

3.1.1 First critical point ①

It's about a transition from a steady-state flow to the beginning of chaos. It can be seen from Fig. 6, a slight difference in the average Nusselt value from 5.115 to 5.093 for an increment in Richardson's number from 6.8 to 6.9. The corresponding contour patterns and isotherms have been plotted in Fig. 5, which shows a slight difference in the flow domain around this first instability. There is a start of change towards an unsymmetrical structure suddenly appearing in the cavity. Adjacent fluid layers have been created at the vertical sides under the shear effect of sliding lids, additionally to an anticlockwise cell that gradually got bigger was formed at the right half of the enclosure. It should be noted from this figure that the effect of a low Richardson's number on the distribution of isotherms is not that much due to thepredominance of lids velocity over the buoyancy forces.

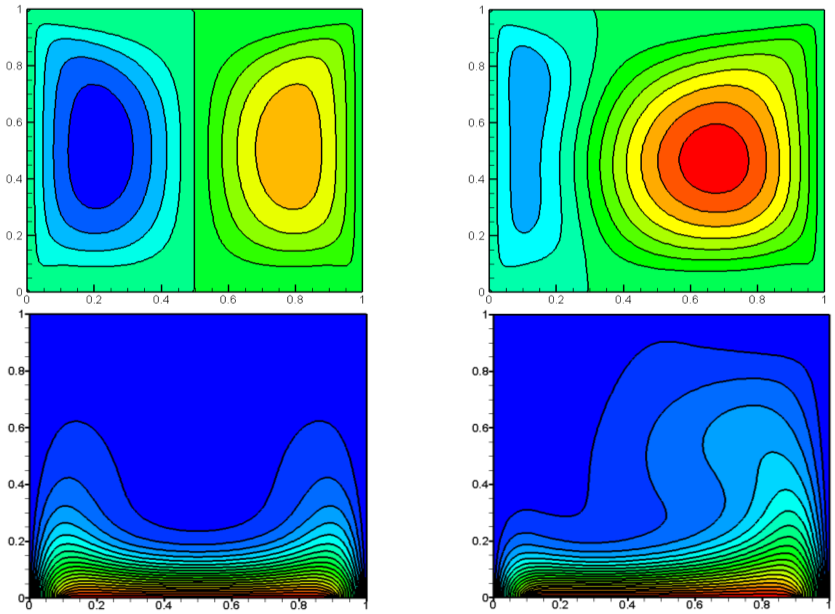

Fig 5. Distribution of flow fields (upper row) and isotherms (bottom) for *Ri*=6.8 (left) and *Ri*=6.9 (right)

The heat exchange through the heated part of this first instability for these two representative values of Richardson number is displayed easily in Fig. 6. In general, the transfer rate decreases suddenly during the first moments. Then, it decreases regularly before attaining a constant value $\overline{Nu}$ =5.115 for *Ri*=6.8. However, it decreases progressively at τ=200 when *Ri*=6.9 and becomes stable towards a fixed value $\overline{Nu}$ =5.093 around τ=240.

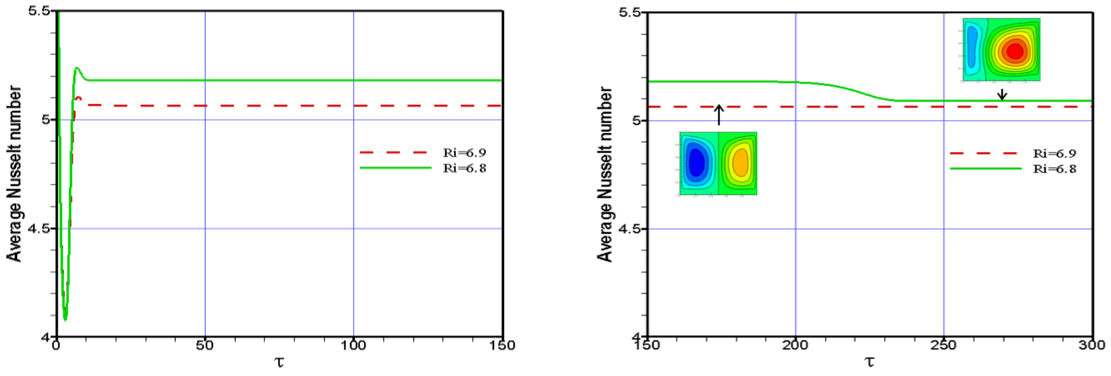

Fig 6. Average Nusselt number evolution for *Ri*=6.8 and *Ri*=6.9 at different time steps

3.1.2 Second critical point ②

It’shighlights a significant change in flow behavior before and after this bifurcation. Indeed, it changes from a pair of counter-rotating rolls with two different shapes and intensities to four symmetrical eddies for the considered values of the same number of mixed regime equal to 11.76 and 11.77, respectively. In this case, the centrally located two cells adjacent to the hot part become denser and thinner, pressing against the other rolls induced by shear forces just towards the moving cell faces (see Fig. 7 at the top right). Here, all of the heat energy at the bottom is symmetrically moved upward in the form of a thermal feather across the central part of the flow domain. From here, we can say that the heat source is dissipated evenly across the sliding walls, and the highest temperatures are located in the central region of the closed body.

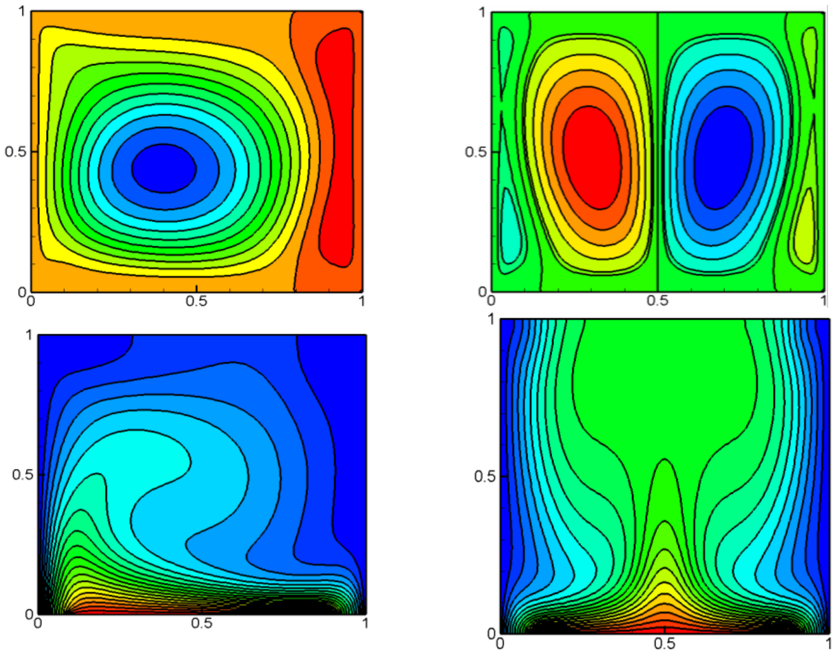

Fig 7. Distribution of flow fields (upper row) and isotherms (bottom) for ***Ri***=11.76 (left) and ***Ri***=11.77 (right)

The effects of both values of Richardson's parameter considered in this case on the heat transfer process are plotted in Fig. 8, designated by the evolution of the average Nusselt number at different time steps. It is shown from this figure that interesting fluctuations occur during the first moments, between 0 and 13 (Fig. 8 on the left). It is also observed that after this disturbance, the obtained value of this parameter decreases steadily, as shown on the right-hand side of Fig. 8, stabilizing at a fixed value of 5.239 when *Ri*=11.77. However, a radical change in flow behavior giving rise to a "bifurcation phenomenon" was observed for the Richardson value of 11.76, resulting in the transition from the first stabilization of $\overline{Nu}$ =5.845 to the second one at $\overline{Nu}$ =5.470. A bifurcation towards a new regime corresponding to the second stabilization begins to occur at τ=120.

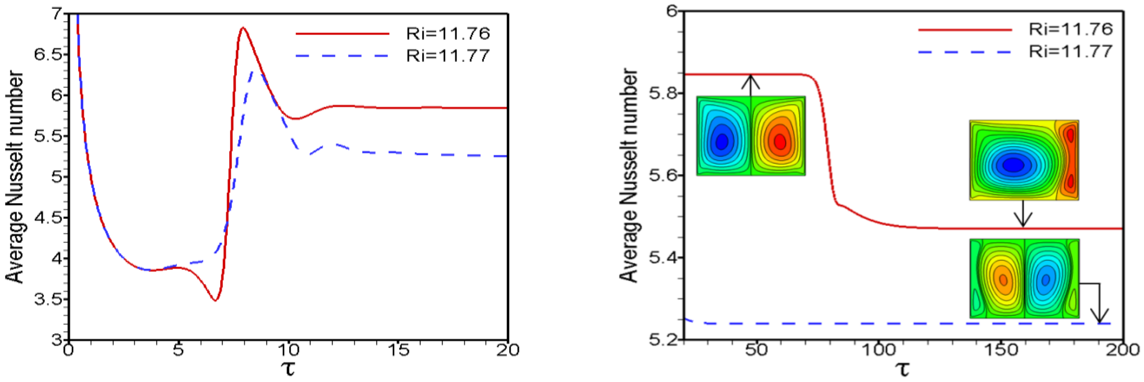

Fig 8. Evolution of Average Nusselt number for ***Ri***=11.76 and ***Ri***=11.77 at different time steps

3.1.3 Third critical point ③

In this case, we revert to an unbalanced flow regime, as shown clearly in Fig. 9. This illustration describes the crucial role of the moving lids in the structure of the flow. There is a significant bifurcation that occurs when the Richardson value increases from 22.7 to 22.8. However, in this scenario, the large anticlockwise circulation eddy has been oriented towards the right side of the enclosure as a result of the interaction between the viscous effect near the moving right and left faces and the buoyancy force induced by the heated portion at the lower wall. This competition plays a significant role in evenly distributing the heat energy along the right wall.

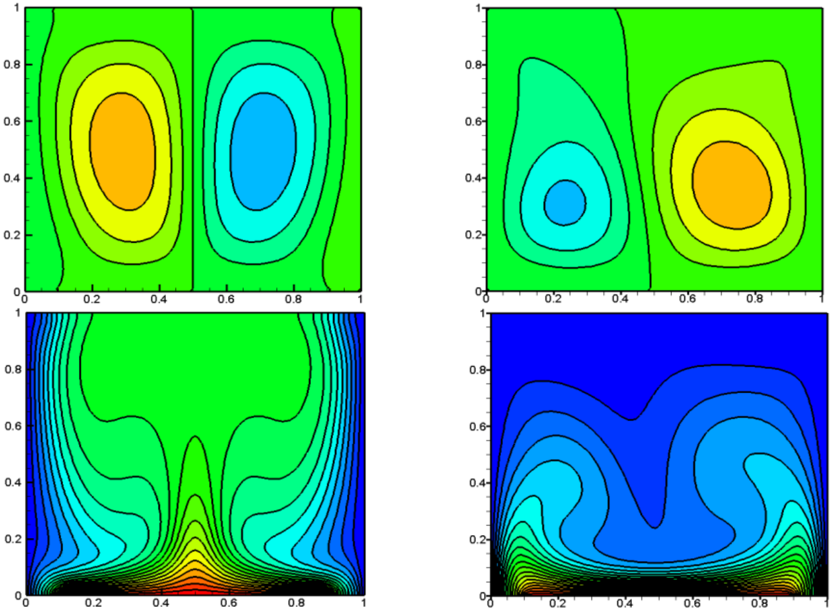

Fig 9. Distribution of flow fields (upper row) and isotherms (bottom) for *Ri*=22.7 (left) and *Ri*=22.8 (right)

Here, it's important to note the progression of the heat transfer rate along the heat source, as depicted in Fig. 10, which characterizes a fourth type of flow regime consisting of two perfectly asymmetric eddies. It's observed from the left side of this figure that the value of this parameter oscillates during the initial moments between 0 and 7, then progressively decreases to stabilize at a constant value ($\overline{Nu}$=6.903) for Ri=22.7. Suddenly, unpredictable fluctuations are presented (see Fig. 10 on the right), gradually subsiding until the second stability is achieved at ($\overline{Nu}$=6.119), characterizing a flow defined by two pairs of identical cells. Meanwhile, for Ri=22.8, the transient heat transfer evolves towards a fixed value of 6.917, indicating a stable development of the flow regime characterized by two perfectly anti-symmetric eddies.

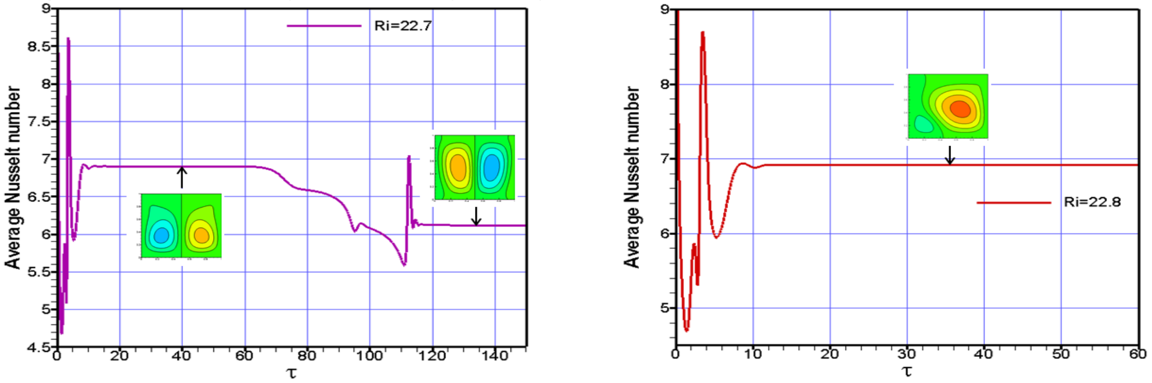

Fig 10. Evolution of Average Nusselt number for *Ri*=22.7 and *Ri*=22.8 at different time steps

3.1.4 Fourth critical point ④

A similar behavior was observed at the final instability point, with the Richardson number between 25.9 and 26. It's evident from Fig. 11 that the corresponding flow patterns and isotherms before and after this critical point were significantly altered. It represents a meaningful bifurcation towards a new type of flow identified by two pairs of symmetrical eddies after having two unbalanced cells that defined the previous state regime. In this instance, the shear forces have sufficient capacity to transport all the heat from below to evenly distribute it towards the center of the confined space. Fig. 12 indicates a sudden change in the rate of heat transfer from 7.081 to 6.344.

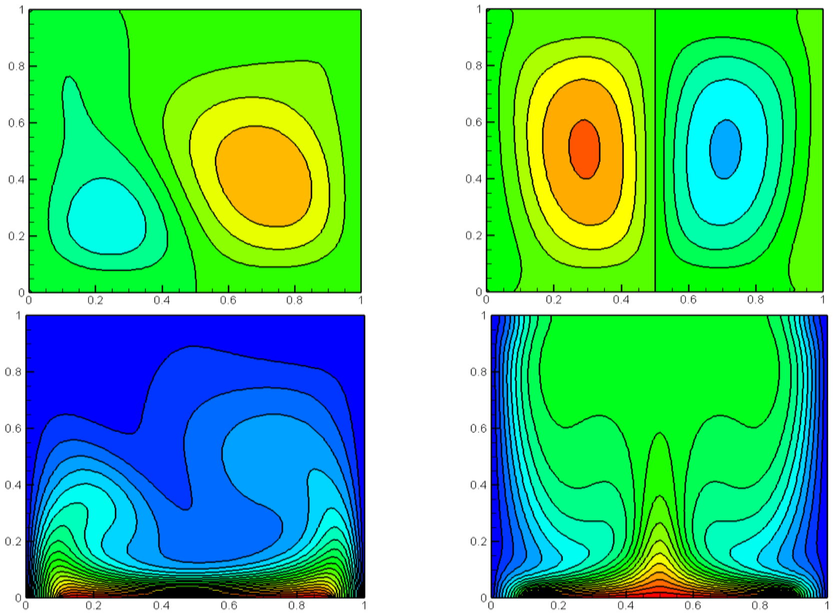

Fig 11. Distribution of flow fields (upper row) and isotherms (bottom) for *Ri*=25.9 (left) and *Ri*=26 (right)

For the cases with values of 25.9 and 26 of the mixed convection parameter, a similar trend to the second bifurcation was also detected. Visual examination of the average rate of heat transfer evolution (Fig. 12) reveals noticeable oscillations at the value of this parameter observed during the first instants (τ< 15). Then, it has been progressively decreased to remain stable at a constant value of 7.081 for *Ri*=25.9 (Fig.12 at the left). Meanwhile, at *Ri*=26, the transient heat transfer evolves towards a fixed value equal to 7.062, showing a stable development of the regime flow which is characterized by two perfectly symmetric eddies. Suddenly, it presented unpredictable fluctuations, which gradually subsided until the second stability was achieved at 6.344, as seen on the right of the same figure, characterizing a flow defined by two pairs of equally identical counter-rotating rolls.

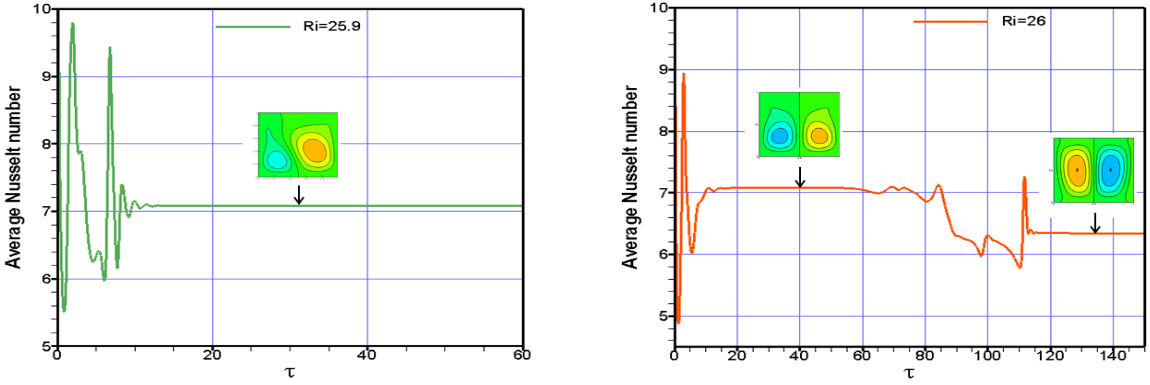

Fig 12. Evolution of Average Nusselt number for *Ri*=25.9 and *Ri*=26 at different time steps

Conclusion

In this paper, a modest contribution to the study of mixed convection in analyzing airflow confined inside a porous substrate is investigated. A part of the substrate, located in the middle of its lower wall, is subjected to a high temperature. Its vertical sides are cooled by a fluid circulating with an ascending velocity. Despite perfectly symmetrical boundary conditions, we have shown that depending on the value of the Richardson number, several different structures of air circulation and temperature gradients can emerge in the considered geometric configuration.The findings indicate that:

- Convective instability may result from the competition between buoyancy source forces and the shear forces caused by the sliding lids.
- We observe four critical points of bifurcation. The first occurs at the transition from a Richardson value of 6.8 to 6.9, while the second one is obtained for values between 11.76 and 11.77. An increment in this parameter from 22.7 to 22.8 leads to the appearance of a third type of change in flow behavior. Subsequently, significant progress toward the final instability phenomenon occurs at Richardson values of 25.9 and 26.

Nomenclature

C_F	– Forchheimer coefficient	ν	– Fluid kinematic viscosity, [m^{2}s^{-1}]
Da	– Darcy number	ρ_f	– Fluid density, [kgm^{-3}]
G	– Gravitational acceleration, [ms-^{1}]	θ	–Dimensionless temperature
Gr	– Grashof number	τ	–Dimensionless time
K	– Permeability of the porous medium, [m^2]	ψ	–Dimensionless stream fuction
l	– length of heat source, [m]	Ψ	– Stream fuction
L	– Enclosure length, [m]	ω	–Dimensionlessvorticity
Nu	– Nusselt number	Ω	–Vorticity
Pr	– Prandtl number		*Subscripts*
Re	– Reynolds number	$\overline{}$	– Average value
Ri	– Richardson number	$_c$	– refers to cold
t	– time	$_e$	– refers to effective property
T	– Temperature, [K]	$_h$	– refers to hot
U,V	– Dimensionless velocity components	$_i$	– refers to X locationof a grid point
V0	– Side walls velocity, [ms-^{1}]	$_j$	– refers to Ylocationof a grid point
X,Y	–Dimensionless coordinates		*Acronyms*
	Greek symbols	CNNs	– Convolutional Neural Networks
α	–Thermal diffusivity of porous medium, [m^{2}s^{-1}]	ED-CNNs	– Encoder-Decoder CNN
β	– Thermal expansion coefficient, [k^{-1}]	ISPH	– Incompressible smoothed Particle
ε	– Dimensionless length of heat source	N.L.O.R	– Non Linear Over Relaxation

References

[1] Mauro,A., Mohamed, S., Three dimensional heat and mass transfer in human eye based on porous medium approach, *International Journal of Heat and Mass Transfer*, *158* (2020), p. 119994

[2] Hewit, D. R., Extract-Air Window Vigorous convection in porous media, *Proceedings A* (The Royal SocietyPublishing), Mathematical, Physical and Engineering Sciences, http://dx.doi.org/10.1098/rspa.2020.0111

[3] Akhila, P. A., *et al*., Analysis of weakly nonlinear Darcy–Brinkman bio-thermal convection in a porous medium under gravity modulation and internal heating effect, *Heliyon, 159* (2024), p. 104615

[4] Roy, N. C., Akter, A., Dual solutions of mixed convective hybrid nanofluid flow over a shrinking cylinder placed in a porous medium, *Heliyon, 09* (2023), p. e22166

[5] Aly, A. M., *et al*., Circular rotation of different structures on natural convection of nanofluid-mobilized circular cylinder cavity saturated with a heterogeneous porous medium, *Heliyon, 09* (2023), p. e22865

[6] Abderrahmane, A., *et al*., MHD Hybrid Nanofluid Mixed Convection Heat Transfer and Entropy Generation in a 3-D Triangular Porous Cavity with Zigzag Wall and Rotating Cylinder, *Mathematics*, https://doi.org/10.3390/math10050769

[7] Mourad, A., *et al*., Numerical Simulations of Magnetohydrodynamics Natural Convection and Entropy Production in a Porous Annulus Bounded by Wavy Cylinder and Koch Snowflake Loaded with Cu–Water Nanofluid, *Micromachines*, https://doi.org/10.3390/mi13020182

[8] Choudhary, P., Ray, R. K., MHD natural convection flow in a porous medium-filled corrugated enclosure: Effect of heat sources with different heights, *International Journal of Thermal Sciences, 196* (2024), p. 108673

[9] Xuan, Z. H., et al., Significance of the natural convection to the heat transfer of porous media: A pore-scale study, *International Journal of Heat and Mass Transfer, 222* (2024), p. 125163

[10] Virupaksha, A. G., et al., Modeling transient natural convection in heterogeneous porous media with Convolutional Neural Networks, *International Journal of Heat and Mass Transfer, 222* (2024), p. 125149

[11] Bazneshin, M. N., *et al*., Significance of the natural convection to the heat transfer of porous media: A pore-scale study, *Case Studies in Thermal Engineering, 50* (2023), p. 103450

[12] Rasool, G., *et al*., Darcy-Forchheimer Flow of Water Conveying Multi-Walled Carbon Nanoparticles through a Vertical Cleveland Z-Staggered Cavity Subject to Entropy Generation, *Micromachines,* https://doi.org/10.3390/mi13050744

[13] Ashraf, M., *et al*., Analysis of the Physical Behavior of the Periodic Mixed-Convection Flow around a Nonconducting Horizontal Circular Cylinder Embedded in a Porous Medium, *Journal of Mathematics*, https://doi.org/10.1155/2021/8839146

[14] Chakingal, M., *et al*., Effect of packing height and location of porous media on heat transfer in a cubical cavity: Are extended Darcy simulations sufficient, *International Journal of Heat and Fluid flow, 84* (2020), p. 108617

[15] Luther, E. E., *et al*., Onset of convective instability in an inclined porous medium, *Physics of fluids, 34* (2022), p. 014104

[16] Kumar, V., *et al*., Vertically oscillated gyrotactic bio-thermal convection in a porous media, *Forces in Mechanics, 09* (2022), p. 100136

[17] Dalila, M., *et al*., Symmetry-Breaking in a Porous Cavity with Moving Side Walls, *International Journal of Engineering Research in Africa, 58* (2022), pp. 45-62

[18] Sangtarash, A., *et al*., A comprehensive investigation of porous media's effects on te performance of photovoltaic hermal system, *Applied Thermal Engineering, 245* (2024), p. 122766

[19] Meria, F. H., *et al*., Impact of porous media on PV/thermal system performance: A short review, *Energy Reports, 11* (2024), pp. 1803- 1819

[20] Mandal, D. K., *et al*., Convective heat transport in a porous wavy enclosure: Nonuniform multy-frequency heating with hybrid nanofluid and magnetic field, *Heliyon, 10* (2024), p. e29846

[21] Peter, F., *et al*., Analizing the MHD bioconvective Eyring—Powell fluid flow over an upright cone/plate surface in a porous medium with activation energy at viscous dissipation, *Computations, 12* (2024), p. 12030048

[22] Zaman, S. U., *et al*., Analysis of heqttrqnsfer in q non-Newtonian nanofluid model with temperature-dependent viscosity flozing though a thin cylinder, *Cases studies in thermal engineering, 54* (2024), p. 104086

[23] Kawamura, T., *et al*.,New Higher-Order Upwind Scheme for Incompressible Navier-Stokes Equations, *Lecture Note in Physics*, 09th Conference on Numerical Method Fluid Dynamics, Springer, Berlin, 1985, Vol. 218, pp. 291-295

[24] Steven, C. C., Applied Numerical Methods With MATLAB for Engineers and Scientists, MC Grow Hill, New York, USA, 1969

[25] Kumar, D. S., *et al*., Analysis of non-darcy Models for mixed convection in a porous cavity using a multigrid approach, *Numerical Heat Transfer, Part A, 56* (2009), pp. 685-708

[26] Iwatsu, R., *et al*.,Mixed convection in a driven cavity with a stable vertical temperature gradient, *International Journal of Heat and Mass Transfer, 36* (1993), pp. 1601-1608

[27] Waheed, M., *et al*.,Mixed convective heat transfer in rectangular enclosure filled with porous media, *Journal of Engineering and Applied Sciencesr, 6* (2011), pp. 47-60

[28] Khanafer, K. M.,Chamkha, A. J., Mixed convection flow in a lid-driven enclosure filled with a fluid-saturated porous medium, *International Journal of Heat and Mass Transfer, 42* (1999), pp. 2465-2481

Submitted: 10.6.2024.
Revised: 4.10.2024.
Accepted: 7.10.2024.